

Point target detection and subpixel position estimation in optical imagery

Vincent Samson, Frédéric Champagnat

*Office National d'Études et de Recherches Aéronautiques,
29, avenue de la division Leclerc, 92322 Châtillon Cedex, France*

Jean-François Giovannelli

*Laboratoire des Signaux et Systèmes,
Supélec, Plateau de Moulon, 91192 Gif-sur-Yvette Cedex, France*

This paper addresses the issue of detecting point objects in a clutter background and estimating their position by image processing. We are interested in the specific context where the object signature significantly varies with its random subpixel location because of aliasing. Conventional matched filter neglects this phenomenon and causes consistent loss of detection performance. Thus, alternative detectors are proposed and numerical results show the improvement brought by approximate and generalized likelihood ratio tests in comparison with pixel matched filtering. We also study the performance of two types of subpixel position estimators. Finally, we put forward the major influence of sensor design on both estimation and point object detection performance. © 2018 Optical Society of America

OCIS codes: 040.1880, 100.5010, 100.0100.

1. Introduction

We tackle the problem of subpixel object detection in image sequences which arises for instance in infrared search and track (IRST) applications. In this context, the target signature is proportional to:

$$s_{\epsilon}[i, j] = \int_{i-0.5}^{i+0.5} \int_{j-0.5}^{j+0.5} h_o(u - \epsilon_1, v - \epsilon_2) du dv. \quad (1)$$

$s_{\epsilon}[i, j]$ represents the percentage of light intensity at pixel (i, j) , $\epsilon = (\epsilon_1, \epsilon_2)$ refers to the object random subpixel position and h_o is the optical point spread function (PSF). According to common sensor design, the energy of the signal component $s = \alpha s_{\epsilon}$ is almost concentrated on a single pixel. However, contrary to the amplitude α which is unknown too, dependence on the location parameter ϵ is highly nonlinear. Its influence in our application is rather significant because of aliasing and unless a velocity model is available, object subpixel position is hardly predictable from frame to frame. Actually, common sensor design leads to an image spot downsampled by almost a factor 5. We can see on Figure 1 the energy loss at central pixel according to subpixel location and the random change in spatial pattern due to aliasing. This phenomenon has a major impact on detection performance as

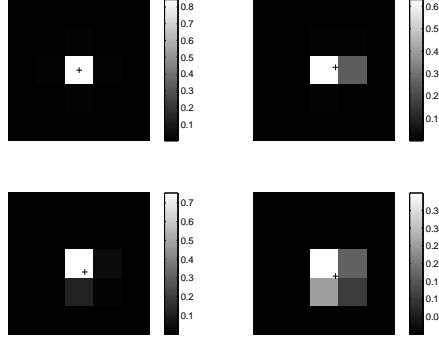


Fig. 1. Examples of image spots for different cross-marked subpixel positions (windows of size 5×5 pixels). Sensor design parameter r_c is set to its common value of 2.44 (see section 3).

shown thereafter. To our knowledge, this pitfall has not been addressed yet in the literature. A prevailing opinion stands that there is no signature information in subpixel objects. Indeed, the different authors dealing with small object detection have concentrated on clutter removing,¹⁻³ multi- or hyper-spectral fusion^{4,5} and multiframe tracking methods.⁶⁻⁸ We focus here on the processing of a single frame. In section 2, we formulate the detection problem in the classical model of a signal in additive Gaussian noise [9, ch.2-4]. When the signal is deterministic, Neyman-Pearson strategy yields the conventional matched filter. In the present case, the signal from the target depends on unknown parameters and we have to deal with a composite hypothesis test. A common procedure is given by the generalized likelihood ratio test. But the “nuisance” parameters α and ϵ can also be considered as random variables with known distributions (some *a priori* density functions in the Bayesian terminology), then the straightforward extension of the likelihood ratio test is to integrate the conditional distribution over α and ϵ . When modelling the signal component as a sample function, we could also think of the class of random signal in noise detection problems, which have essentially been studied in the Gaussian case. Unfortunately, considering s_ϵ as a random vector, its empirical distribution proves to be highly non Gaussian when ϵ is uniformly sampled. For instance, the histogram of the central pixel depicted on Figure 2 shows that a Gaussian fit is not satisfactory at all. In section 3, we define more precisely the optical system model used in our numerical experiments. We consider both a Gaussian white noise and a fractal noise of unknown correlations generated by a standard technique of spectral synthesis. Section 4 is devoted to the position estimation problem, i.e. estimation of parameter ϵ . We propose two estimators that take into account the fact that the signal amplitude α is also unknown. We demonstrate the performance of these estimators in terms of mean square errors. As for the detection problem, we finally illustrate the expected improvement in quality brought by a correctly sampled optics compared to common sensor design.

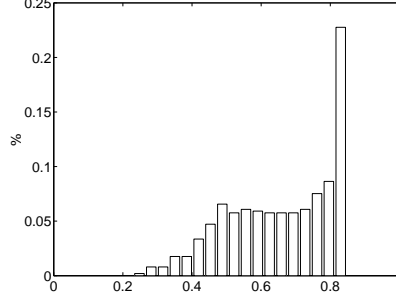


Fig. 2. Empirical distribution of the image-spot central pixel $s_\epsilon[0, 0]$ for a uniformly random position $\epsilon \sim \mathcal{U}_{[-0.5, 0.5]^2}$.

2. Detection problem

We consider a local detection window sliding across the image. The problem is to decide whether an object is present or not at the window central pixel. This is a binary test which typically reads as follows:

$$\begin{cases} H_0 & : \mathbf{z} = \mathbf{n} \\ H_1 & : \mathbf{z} = \alpha \mathbf{s}_\epsilon + \mathbf{n} \end{cases} \quad (2)$$

where \mathbf{z} is the vector collecting the window data, $\mathbf{s} = \alpha \mathbf{s}_\epsilon$ is the object response (signal vector) and \mathbf{n} the additive Gaussian noise. The signature shape is known and deterministic, so that \mathbf{s} only depends on the two unknown parameters $\alpha \in \mathbb{R}$ and $\epsilon \in \mathcal{E} = [-0.5, 0.5]^2$. The noise vector \mathbf{n} is supposed to be centered (in practice we first remove the empirical mean from the data) with a known or previously estimated covariance matrix \mathbf{R} . Thus, if we assume that \mathbf{n} is independent from \mathbf{s} , the following conditional distributions are Gaussian:

$$\begin{cases} p(\mathbf{z}|H_0) & \sim \mathcal{N}(0, \mathbf{R}) \\ p(\mathbf{z}|H_1, \alpha, \epsilon) & \sim \mathcal{N}(\alpha \mathbf{s}_\epsilon, \mathbf{R}) \end{cases} \quad (3)$$

Let first assume that parameters α and ϵ are given. The problem amounts to a simple hypothesis test which is to detect a deterministic signal in a Gaussian noise. The Neyman-Pearson strategy or likelihood ratio test (LRT) is given by:

$$\frac{p(\mathbf{z}|H_1, \alpha, \epsilon)}{p(\mathbf{z}|H_0)} \underset{H_0}{\overset{H_1}{>}} \text{threshold} \quad (4)$$

It is equivalent to classical matched filtering which simply compares the statistic $\alpha \mathcal{T}_\epsilon(\mathbf{z}) = \alpha \mathbf{s}_\epsilon^t \mathbf{R}^{-1} \mathbf{z}$ with some threshold.

A. Pixel matched filtering

The exact object location being unknown in practice, we could assume by default that $\epsilon = \epsilon_0 = [0, 0]$, i.e. the object is at the center of the pixel, whereas the true location

would correspond to $\epsilon = \epsilon^*$. Thus, the detector which consists in thresholding the pixel matched filter (PMF) $\alpha \mathcal{T}_{\epsilon_0}(z)$ is optimum provided $\epsilon^* = \epsilon_0$. Otherwise it is mismatched and therefore suboptimum. Since conditional distributions of $\mathcal{T}_{\epsilon_0}(z)$ under each assumption are Gaussian, we easily get the expression of the probability of detection P_d and of false alarm P_{fa} . Corresponding receiver operating characteristic (ROC) curves for critical values of ϵ^* are depicted on Figure 3. They clearly show that the PMF performances are significantly worse as ϵ_0 differs from ϵ^* . But beyond extreme situations (related to a true target location between two or four pixels instead of the center), the “mean curve” represents the average statistics over uniformly random positions. Compared to the ideal curve, we can see that the price paid if one neglects the random location is rather high even at favorable signal-to-noise ratio. For a SNR of 15dB and at a P_{fa} of 10^{-4} , probability of detection decreases from nearly 1 to 0.8.

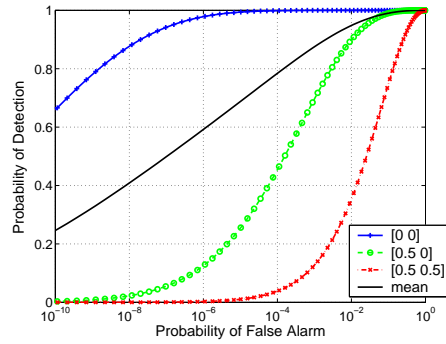


Fig. 3. Examples of pixel matched filter theoretical ROC curves for $\epsilon^* = \epsilon_0$ in blue (ideal curve), $\epsilon^* \neq \epsilon_0$ in green and red (worst case), and finally the mean curve in black for uniformly sampled ϵ^* (SNR = 15dB).

The object response also depends (linearly this time) on the amplitude α , which is generally unknown. Yet, assuming strictly positive amplitude, we see that whatever $\alpha > 0$, thresholding $\alpha \mathcal{T}_{\epsilon_0}(z)$ gives the same ROC curve as thresholding $\mathcal{T}_{\epsilon_0}(z)$. Without any assumption on α , a classical solution is to estimate it by maximum likelihood (ML). Indeed under the Gaussian noise assumption, the optimum in α for a given ϵ is explicit:

$$\begin{aligned} \hat{\alpha}(\epsilon) &= \arg \max_{\alpha \in \mathbb{R}} p(z|H_1, \alpha, \epsilon) \\ &= \arg \min_{\alpha \in \mathbb{R}} \{ (z - \alpha s_\epsilon)^t \mathbf{R}^{-1} (z - \alpha s_\epsilon) \} \\ &= \frac{s_\epsilon^t \mathbf{R}^{-1} z}{s_\epsilon^t \mathbf{R}^{-1} s_\epsilon} \end{aligned} \quad (5)$$

and then the “generalized” pixel matched filter (referred to as GPMF) is equal to

$$\hat{\alpha}(\epsilon_0) \mathcal{T}_{\epsilon_0}(z) = \frac{|s_{\epsilon_0}^t \mathbf{R}^{-1} z|^2}{s_{\epsilon_0}^t \mathbf{R}^{-1} s_{\epsilon_0}}. \quad (6)$$

B. Subpixel detectors

Our aim is to build refined detectors that improve performance of the above GPMF in taking into account the variability of the object signature due to its random subpixel location. Several solutions may be used. We first recall the most popular one.

1. Generalized likelihood ratio test

ML estimation of the two unknown parameters leads to the generalized likelihood ratio test (GLRT):

$$\begin{aligned}\mathcal{L}_g(\mathbf{z}) &= \frac{\max_{(\alpha, \epsilon)} p(\mathbf{z}|\mathbf{H}_1, \alpha, \epsilon)}{p(\mathbf{z}|\mathbf{H}_0)} \\ &= \frac{p(\mathbf{z}|\mathbf{H}_1, \hat{\alpha}_{\text{ML}}, \hat{\epsilon}_{\text{ML}})}{p(\mathbf{z}|\mathbf{H}_0)} \begin{matrix} > \\ < \end{matrix} \text{threshold.}\end{aligned}\tag{7}$$

It consists in estimating the amplitude α and the possible object location ϵ by computing:

$$\begin{aligned}\hat{\epsilon}_{\text{ML}} &= \arg \max_{\epsilon \in \mathcal{E}} p(\mathbf{z}|\mathbf{H}_1, \hat{\alpha}(\epsilon), \epsilon) \\ &= \arg \max_{\epsilon \in \mathcal{E}} \left\{ \frac{|\mathbf{s}_{\epsilon}^t \mathbf{R}^{-1} \mathbf{z}|^2}{\mathbf{s}_{\epsilon}^t \mathbf{R}^{-1} \mathbf{s}_{\epsilon}} \right\},\end{aligned}\tag{8}$$

then thresholding the estimated filter $\hat{\alpha}_{\text{ML}} \mathcal{T}_{\hat{\epsilon}_{\text{ML}}}(\mathbf{z})$ where $\hat{\alpha}_{\text{ML}} = \hat{\alpha}(\hat{\epsilon}_{\text{ML}})$ is given by equation (5):

$$\hat{\alpha}_{\text{ML}} \mathcal{T}_{\hat{\epsilon}_{\text{ML}}}(\mathbf{z}) = \frac{|\mathbf{s}_{\hat{\epsilon}_{\text{ML}}}^t \mathbf{R}^{-1} \mathbf{z}|^2}{\mathbf{s}_{\hat{\epsilon}_{\text{ML}}}^t \mathbf{R}^{-1} \mathbf{s}_{\hat{\epsilon}_{\text{ML}}}}.\tag{9}$$

2. Exact likelihood ratio test

In a Bayesian approach, we propose to consider the two unknown parameters α and ϵ as realizations of independent random variables with given probability density functions $p(\alpha)$ and $p(\epsilon)$. Then the optimal procedure is the exact likelihood ratio test (ELRT).

To compute the density function of data under \mathbf{H}_1 and to get the likelihood ratio, we have to integrate the conditional density $p(\mathbf{z}|\mathbf{H}_1, \alpha, \epsilon)$ over prior distributions of the nuisance random parameters α and ϵ . The likelihood ratio can be expressed as:

$$\mathcal{L}(\mathbf{z}) = \frac{p(\mathbf{z}|\mathbf{H}_1)}{p(\mathbf{z}|\mathbf{H}_0)} = \frac{\int_{\mathcal{E}} \int_{\mathbb{R}} p(\mathbf{z}|\mathbf{H}_1, \alpha, \epsilon) p(\alpha) p(\epsilon) d\alpha d\epsilon}{p(\mathbf{z}|\mathbf{H}_0)}.\tag{10}$$

Given prior distributions $p(\alpha)$ and $p(\epsilon)$, $\mathcal{L}(\mathbf{z})$ is the optimal Neyman-Pearson test whenever α and ϵ really satisfy the models $p(\alpha)$ and $p(\epsilon)$. By default we choose a “non-informative” prior for α and we adopt a uniform distribution inside the pixel for ϵ , which seems to be quite a reasonable assumption for the subpixel target position. So we get:

$$\mathcal{L}(\mathbf{z}) \propto \int_{\mathcal{E}} \frac{1}{\sqrt{\mathbf{s}_{\epsilon}^t \mathbf{R}^{-1} \mathbf{s}_{\epsilon}}} \exp \left\{ \frac{|\mathbf{s}_{\epsilon}^t \mathbf{R}^{-1} \mathbf{z}|^2}{2 \mathbf{s}_{\epsilon}^t \mathbf{R}^{-1} \mathbf{s}_{\epsilon}} \right\} d\epsilon.\tag{11}$$

Unfortunately, because of intricate nonlinear dependence of \mathbf{s}_{ϵ} on ϵ , explicit integration over ϵ appears to be not tractable and probability distribution of $\mathcal{L}(\mathbf{z})$ is not as simple as the one of $\mathcal{T}_{\epsilon_0}(\mathbf{z})$. A quadrature approximation is required to compute $\mathcal{L}(\mathbf{z})$ whereas derivation of its density requires Monte-Carlo simulations.

3. Approximate likelihood ratio test

In equation (11), the double integral over ϵ can be approximated up to any desired accuracy using some quadrature rule and evaluating the integrand $f(\epsilon|z)$ at discrete samples $\epsilon_k \in \mathcal{E} = [-0.5, 0.5]^2$. But, for sake of computational efficiency, we propose to use a coarsest approximation of the likelihood ratio (ALRT) based on a bidimensional trapezoidal rule which only involves the 9 half-pixel positions.

4. Subspace model

One alternative to this probabilistic viewpoint can be built on a geometric approach that restricts the signal vector $\mathbf{s} = \alpha \mathbf{s}_\epsilon$ to vary in some P -dimensional subspace, with P lower than the vector size.¹⁰ The observed data under H_1 are rewritten as:

$$\mathbf{z} \simeq \mathbf{S}\mathbf{a} + \mathbf{n} = \sum_{p=1}^P a_p \mathbf{s}_p + \mathbf{n}, \quad (12)$$

where the structural matrix \mathbf{S} is formed by P independent vectors \mathbf{s}_p . Coefficients a_p of the linear combination are the new parameters that describe the signal variability. Thanks to linearity, ML estimation of vector \mathbf{a} has an explicit solution (which is identical to the least squares estimator):

$$\hat{\mathbf{a}}_{\text{ML}} = (\mathbf{S}^t \mathbf{R}^{-1} \mathbf{S})^{-1} \mathbf{S}^t \mathbf{R}^{-1} \mathbf{z} \quad (13)$$

and GLRT amounts to threshold the following statistic:

$$\mathcal{D}(\mathbf{z}) = \mathbf{z}^t \mathbf{R}^{-1} \mathbf{S} (\mathbf{S}^t \mathbf{R}^{-1} \mathbf{S})^{-1} \mathbf{S}^t \mathbf{R}^{-1} \mathbf{z}. \quad (14)$$

Matrix \mathbf{S} only depends on ϵ , α being a scale parameter. In practice, it is identified by discretizing \mathcal{E} , making a singular value decomposition and retaining the singular vectors \mathbf{s}_p corresponding to the P greatest singular values. We choose $P = 1$ which gives better results than higher orders. Therefore under hypothesis H_1 , $\mathbf{z} \simeq a_1 \mathbf{s}_1 + \mathbf{n}$ and $\mathcal{D}(\mathbf{z})$ is identical to GPMF with \mathbf{s}_1 replacing \mathbf{s}_{ϵ_0} .

3. Application to optical imagery

A. Optical system

In our application, we can model the imaging system by a diffraction-limited, unaberrated optics with circular aperture and incoherent illumination.^{11,12} The object signal pattern \mathbf{s}_ϵ is then given by the integration of h_o on each pixel (see equation 1), where h_o is the radial point spread function (PSF) defined by the Airy disk:

$$h_o(u, v) = \frac{1}{\pi} \left[\frac{J_1(\pi \rho r_c)}{\rho} \right]^2, \quad \rho = \sqrt{u^2 + v^2}. \quad (15)$$

J_1 is the Bessel function of the first kind and $r_c = \nu_c / \nu_s$ designates the normalized cut-off frequency (ν_s is the sampling frequency and $\nu_c = D / \lambda$ is the radial cut-off frequency defined by the ratio of the lens aperture diameter D over the wavelength λ). Figure 4 depicts the two-dimensional PSF and a slice along one diameter, as well as their Fourier transform.

Common sensor design uses $r_c = 2.44$ so that the pixel size is equal to the width of the main lobe of the PSF. However, this implies a downsampling factor of $\nu_n/\nu_s = 2r_c = 4.88$ (where $\nu_n = 2\nu_c$ is the Nyquist frequency). In the following section, we present some numerical results of detection performance considering this classical sensor design. Examples of image spots \mathbf{s}_ϵ have been represented on Figure 1 for different values of ϵ .

Remark 1 *We have the following property:*

$$\sum_{(i,j) \in \mathbb{Z}^2} \mathbf{s}_\epsilon[i,j] = \int_{\mathbb{R}^2} h_o(u,v) du dv = 1.$$

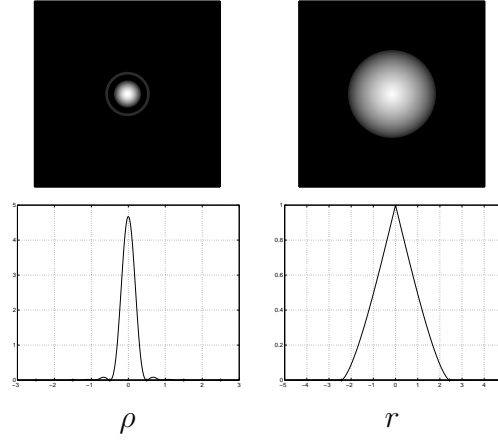


Fig. 4. *Left*: radial point spread function $h_o(u,v)$ on the top and slice along a diameter on the bottom. *Right*: corresponding optical transfer function $\tilde{h}_o(\nu_u, \nu_v)$ and slice along a diameter ($r_c = 2.44$).

B. Numerical results

Performances of the five classes of detectors have been compared in terms of ROC curves: GPMF, GLRT on α and ϵ , ELRT, ALRT and finally GLRT with the subspace model denoted SM-GLRT. Probabilities of detection and false alarm are deduced from the empirical distributions of these statistics under each hypothesis by generating samples of Gaussian noise \mathbf{n} and uniformly distributed ϵ in $\mathcal{E} = [-0.5, 0.5]^2$. The amplitude is assumed to be unknown but set to a constant value α in the simulations since we have no information about a reliable prior distribution $p(\alpha)$.

We first consider the case of a Gaussian white noise $\mathbf{n} \sim \mathcal{N}(0, \sigma^2)$. The signal-to-noise ratio is then defined by:

$$\text{SNR} = 10 \log_{10} \left(\frac{\alpha^2 E}{\sigma^2} \right) \quad (16)$$

$$\text{with } E = \int_{\mathcal{E}} \sum_{(i,j) \in \mathbb{Z}^2} (\mathbf{s}_\epsilon[i,j])^2 d\epsilon$$

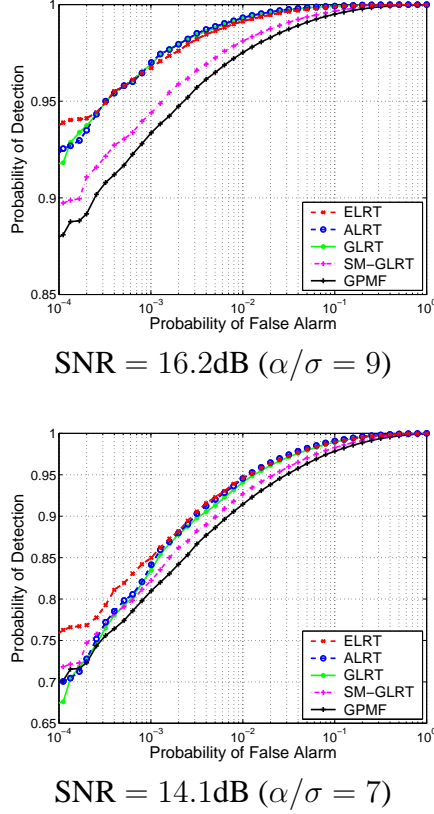


Fig. 5. Empirical ROC curves in the Gaussian white noise case with common sensor design ($r_c = 2.44$).

For common sensor design ($r_c = 2.44$), the average energy of the image spot is $E \simeq 0.52$. The ROC curves are depicted on Figure 5 for two different SNR. It shows that the GLRT, the ELRT (actually, a refined approximation of it) and the coarse approximation ALRT give significantly better performance than the SM-GLRT and GPMF. We also see that the performance gain is greater for high SNR whereas it tends to be rather small for low SNR and low probability of false alarm. Conversely, if the latter detectors are computationally cheap, including the ALRT, this is not so for the GLRT and the ELRT, which are much more intensive.

As complementary results, we have tested the five detectors on a fractal background image generated by a variant of the ppmforge software¹. The synthesis algorithm depends on the auto-similarity parameter H called Hurst parameter and which is set to 0.7 in this experiment. The resulting image depicted on Figure 6 is a realistic simulation of a cloud scene. The covariance matrix \mathbf{R} of this stationary background is estimated by the empirical correlations on the whole image. We then compute the performance of the different detectors for a given target amplitude as illustrated on Figure 7. The ROC curves look quite

¹<http://h30097.www3.hp.com/demos/oss/man-html/man1/ppmforge.1.html>

different from the white noise case but we notice again that the GLRT, ELRT and ALRT have similar performance and provide a significant detection gain in comparison with the GPMF or the SM-GLRT.

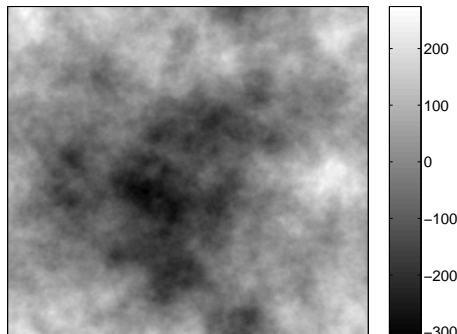


Fig. 6. Simulation of a cloud fractal image of 200×200 pixels (Hurst parameter $H = 0.7$).

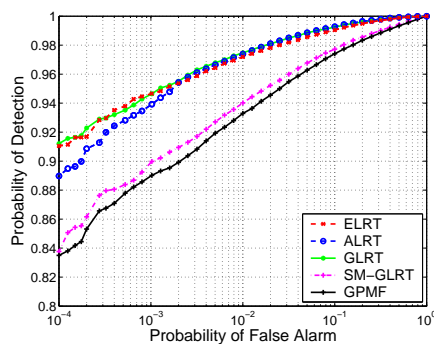


Fig. 7. Empirical ROC curves obtained on the fractal image of Figure 6 for a true (but assumed unknown) target amplitude $\alpha = 60$ gray levels.

C. Influence of the optics

Besides the perfecting and evaluation of subpixel detectors, one additional motivation of this work is to analyze the influence of aliasing on detection performance. This is the reason why we have also tested the detectors on a correctly sampled optics in order to compare their performances with those obtained using a common sensor design. In the correctly sampled design, the focal plane is sampled at Nyquist frequency (implying a denser sensor array or a smaller lens diameter) so that aliasing is suppressed. Parameter r_c of the PSF is equal to 0.5 and the signal energy is now spread over several pixels ($E \simeq 0.08$). By

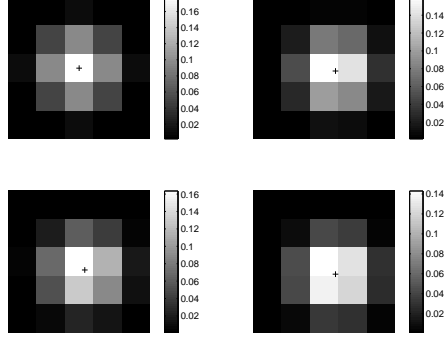


Fig. 8. Examples of image spots corresponding to a correctly sampled optics ($r_c = 0.5$) to be compared to those of Figure 1.

comparison, Figure 8 presents the examples of image spots corresponding to such a design. Detection performances are depicted on Figure 9 on the right for a SNR of 15dB. We see that improved detection has just a moderate impact in this situation. The five detectors have a quite similar behavior but at the same SNR they perform much better than in the aliased case. The gain in P_{fa} amounts at least to a factor 10 for all the detectors. Such a result speaks in favour of using a denser focal plane for point target detection.

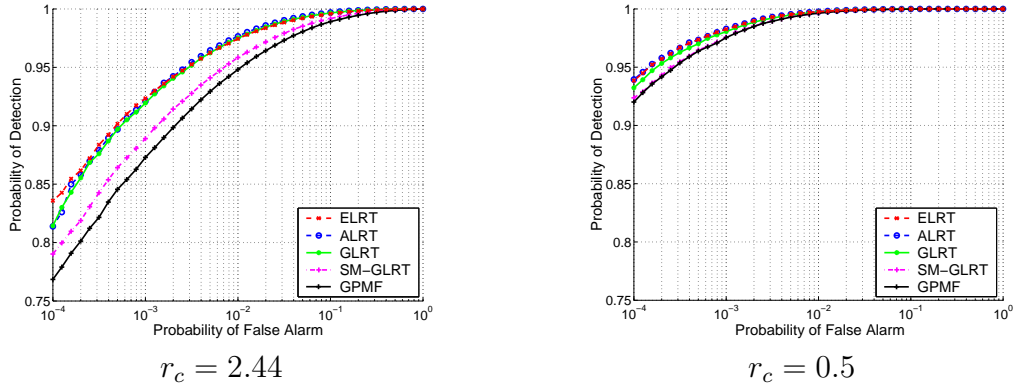


Fig. 9. Empirical ROC curves in the Gaussian white noise case for a same SNR = 15dB, with common sensor design on the left ($r_c = 2.44$) compared to a correctly sampled optics on the right ($r_c = 0.5$).

4. Performance of subpixel position estimators

Up to now we have focused on the detection strategy. In a second step, once a potential target is detected on a given pixel, we are also interested in accurate estimation of its subpixel

position. Such a problem has already been addressed, in particular for star position estimation in astronomical applications.¹³ Several types of estimators are possible. We consider here the maximum likelihood (ML) estimator and following the Bayesian approach introduced previously the posterior mean (PM). It is important to note that the signal amplitude α is also unknown and therefore we have to estimate it or integrate over it. Indeed it is not valid to suppose that the amplitude is known in the context of IRST.

The ML estimator of ϵ is given in equation (8) by replacing α with its estimate $\hat{\epsilon}$. Actually, $\hat{\epsilon}_{\text{ML}}$ and $\hat{\alpha}_{\text{ML}} = \hat{\alpha}(\hat{\epsilon}_{\text{ML}})$ are identical to joint maximum *a posteriori* (MAP) estimators with non-informative priors on the two parameters.

The PM estimator is defined as:

$$\hat{\epsilon}_{\text{PM}} = \int_{\mathcal{E}} \epsilon p(\epsilon | H_1, \mathbf{z}) d\epsilon \quad (17)$$

where the posterior law is deduced from Bayes' rule:

$$\begin{aligned} p(\epsilon | H_1, \mathbf{z}) &= \frac{p(\mathbf{z} | H_1, \epsilon) p(\epsilon)}{p(\mathbf{z} | H_1)} \\ &= \frac{p(\epsilon)}{p(\mathbf{z} | H_1)} \int_{\mathbb{R}} p(\mathbf{z} | H_1, \alpha, \epsilon) p(\alpha) d\alpha. \end{aligned} \quad (18)$$

So, we have to integrate over α and then over ϵ . As previously we consider a diffuse *a priori* on \mathbb{R} for α and a uniform law on \mathcal{E} for ϵ . We get the following expression in the same way as for the likelihood ratio in equation (11):

$$p(\epsilon | H_1, \mathbf{z}) \propto \frac{1}{\sqrt{\mathbf{s}_\epsilon^t \mathbf{R}^{-1} \mathbf{s}_\epsilon}} \exp \left\{ \frac{|\mathbf{s}_\epsilon^t \mathbf{R}^{-1} \mathbf{z}|^2}{2 \mathbf{s}_\epsilon^t \mathbf{R}^{-1} \mathbf{s}_\epsilon} \right\}. \quad (19)$$

We have studied the performance of these two estimators in terms of average mean square error (MSE). In practice, the optimization or the integration over ϵ are approximated numerically by considering a finite discrete grid of 20×20 values $\epsilon_k \in \mathcal{E}$. Given a true position ϵ^* , bias and variance of an estimator $\hat{\epsilon}$ are estimated thanks to Monte-Carlo simulations. We consider the case of a Gaussian white noise and we vary the signal-to-noise ratio. Figure 10 on the left compares ML and PM estimators to the pixel estimator which assumes by default that the target location is at the center of the pixel ($\hat{\epsilon} = (0, 0)$) and whose MSE is equal to $1/12$. At favorable SNR, the two subpixel estimators are far better than the default estimator but the gain decreases when the noise becomes important. For a SNR of 15dB, the ML yields an error similar to the default estimator while the PM notably has a twice smaller error. By comparison, Figure 10 on the right shows the estimation performances obtained in the unaliased case ($r_c = 0.5$) for equivalent signal-to-noise ratios. ML and PM logically perform better since the signal is correctly sampled.

5. Conclusion and future work

We have presented the detection problem of subpixel objects embedded in additive Gaussian noise. Subpixel location and signal amplitude are assumed to be unknown. Unknown subpixel location has a great influence on detection performance in the aliased case while

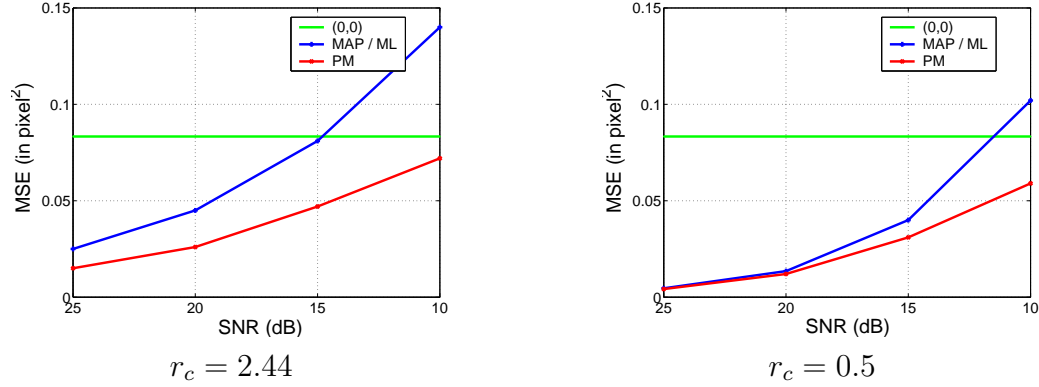


Fig. 10. Average mean square errors (MSE) of position estimators in the Gaussian white noise case with common sensor design on the left ($r_c = 2.44$) compared to a correctly sampled optics on the right ($r_c = 0.5$).

conventional matched filter neglects it. Thus, we derived four types of improved detectors from the likelihood ratio: the GLRT, the ELRT, the ALRT and the SM-GLRT. We have illustrated their performance in comparison with the more classical GPMF. Numerical results for both white and correlated noise cases show that the ELRT, the ALRT and the GLRT are competitive whereas the SM-GLRT does not reach the same quality but slightly improves the performance of the GPMF too. The ALRT seems to be a good trade-off since it is not as computationnally demanding as the ELRT and the GLRT. Moreover the performance gain proves to be only moderate in the case of unaliased optics. This conclusion has important consequence in sensor design: it suggests that the popular design of a pixel covering exactly the main lobe of the Airy disk is not optimum for point object detection. Future work consists in studying the robustness of these detectors to real data and the way we can take into account non Gaussian distributions of background noise. As far as the position estimation problem is concerned, we have demonstrated prospective gains that must also be confirmed on more realistic data.

References

1. C. D. Wang, “Adaptive spatial/temporal/spectral filters for background clutter suppression and target detection,” *Optical Engineering*, vol. 21, pp. 1033–1038, Dec. 1982.
2. A. Margalit, I. S. Reed, and R. M. Gagliardi, “Adaptive optical target detection using correlated images,” *IEEE Transactions on Aerospace and Electronic Systems*, vol. 21, pp. 394–405, May 1985.
3. T. Soni, J. R. Zeidler, and W. H. Ku, “Performance evaluation of 2-D adaptive prediction filters for detection of small objects in image data,” *IEEE Transactions on Image Processing*, vol. 2, pp. 327–340, July 1993.
4. X. Yu, L. E. Hoff, I. S. Reed, A. M. Chen, and L. B. Stotts, “Automatic target detection and recognition in multiband imagery : a unified ML detection and estimation

- approach,” *IEEE Transactions on Image Processing*, vol. 6, pp. 143–156, Jan. 1997.
5. E. A. Ashton, “Detection of subpixel anomalies in multispectral infrared imagery using an adaptive Bayesian classifier,” *IEEE Transactions on Geoscience and Remote Sensing*, vol. GE-36, pp. 506–517, Mar. 1998.
 6. I. S. Reed, R. M. Gagliardi, and H. M. Shao, “Application of three-dimensional filtering to moving target detection,” *IEEE Transactions on Aerospace and Electronic Systems*, vol. 19, pp. 898–905, Nov. 1983.
 7. S. D. Blostein and T. S. Huang, “Detecting small, moving objects in image sequences using sequential hypothesis testing,” *IEEE Transactions on Signal Processing*, vol. 39, pp. 1611–1629, July 1991.
 8. J. M. Mooney, J. Silverman, and C. E. Caefer, “Point target detection in consecutive frame staring infrared imagery with evolving cloud clutter,” *Optical Engineering*, vol. 34, pp. 2772–2784, Sept. 1995.
 9. H. L. Van Trees, *Detection, estimation and modulation theory*. Part1, New York: Wiley, John, 1968.
 10. D. Manolakis and G. Shaw, “Detection algorithms for hyperspectral imaging applications,” *Signal Processing Magazine*, vol. 19, pp. 29–43, Jan. 2002.
 11. J. W. Goodman, *Introduction à l’optique de Fourier et à l’holographie*. Paris: Masson, 1972.
 12. R. C. Hardie, K. J. Barnard, J. G. Bognar, E. E. Armstrong, and E. A. Watson, “High-resolution image reconstruction from a sequence of rotated and translated frames and its application to an infrared imaging system,” *Optical Engineering*, vol. 37, pp. 247–260, Jan. 1998.
 13. K. A. Winick, “Cramer-Rao lower bounds on the performance of charge-coupled-device optical position estimators,” *Journal of the Optical Society of America A*, vol. 3, pp. 1809–1815, Nov. 1986.

Point target detection and subpixel position estimation in optical imagery

Vincent Samson, Frédéric Champagnat

*Office National d'Études et de Recherches Aérospatiales,
29, avenue de la division Leclerc, 92322 Châtillon Cedex, France*

Jean-François Giovannelli

*Laboratoire des Signaux et Systèmes,
Supélec, Plateau de Moulon, 91192 Gif-sur-Yvette Cedex, France*

This paper addresses the issue of detecting point objects in a clutter background and estimating their position by image processing. We are interested in the specific context where the object signature significantly varies with its random subpixel location because of aliasing. Conventional matched filter neglects this phenomenon and causes consistent loss of detection performance. Thus, alternative detectors are proposed and numerical results show the improvement brought by approximate and generalized likelihood ratio tests in comparison with pixel matched filtering. We also study the performance of two types of subpixel position estimators. Finally, we put forward the major influence of sensor design on both estimation and point object detection performance. © 2018 Optical Society of America

1. Introduction

We tackle the problem of subpixel object detection in image sequences which arises for instance in infrared search and track (IRST) applications. In this context, the target signature is proportional to:

$$\mathbf{s}_\epsilon[i, j] = \int_{i-0.5}^{i+0.5} \int_{j-0.5}^{j+0.5} h_o(u - \epsilon_1, v - \epsilon_2) du dv. \quad (1)$$

$\mathbf{s}_\epsilon[i, j]$ represents the percentage of light intensity at pixel (i, j) , $\epsilon = (\epsilon_1, \epsilon_2)$ refers to the object random subpixel position and h_o is the optical point spread function (PSF). According to common sensor design, the energy of the signal component $\mathbf{s} = \alpha \mathbf{s}_\epsilon$ is almost concentrated on a single pixel. However, contrary to the amplitude α which is unknown too, dependence on the location parameter ϵ is highly nonlinear. Its influence in our application is rather significant because of aliasing and unless a velocity model is available, object subpixel position is hardly predictable from frame to frame. Actually, common sensor design leads to an image spot downsampled by almost a factor 5. We can see on Figure 1 the energy loss at central pixel according to subpixel location and the random change in spatial pattern due to aliasing. This phenomenon has a major impact on detection performance as

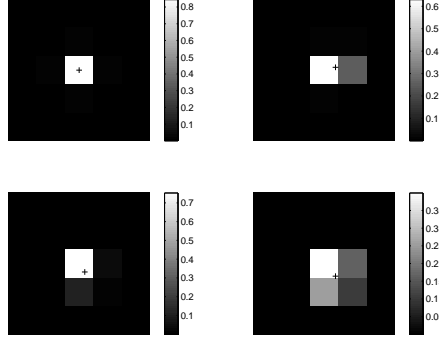


Fig. 1. Examples of image spots for different cross-marked subpixel positions (windows of size 5×5 pixels). Sensor design parameter r_c is set to its common value of 2.44 (see section 3).

shown thereafter. To our knowledge, this pitfall has not been addressed yet in the literature. A prevailing opinion stands that there is no signature information in subpixel objects. Indeed, the different authors dealing with small object detection have concentrated on clutter removing,¹⁻³ multi- or hyper-spectral fusion^{4,5} and multiframe tracking methods.⁶⁻⁸ We focus here on the processing of a single frame. In section 2, we formulate the detection problem in the classical model of a signal in additive Gaussian noise [9, ch.2-4]. When the signal is deterministic, Neyman-Pearson strategy yields the conventional matched filter. In the present case, the signal from the target depends on unknown parameters and we have to deal with a composite hypothesis test. A common procedure is given by the generalized likelihood ratio test. But the “nuisance” parameters α and ϵ can also be considered as random variables with known distributions (some *a priori* density functions in the Bayesian terminology), then the straightforward extension of the likelihood ratio test is to integrate the conditional distribution over α and ϵ . When modelling the signal component as a sample function, we could also think of the class of random signal in noise detection problems, which have essentially been studied in the Gaussian case. Unfortunately, considering s_ϵ as a random vector, its empirical distribution proves to be highly non Gaussian when ϵ is uniformly sampled. For instance, the histogram of the central pixel depicted on Figure 2 shows that a Gaussian fit is not satisfactory at all. In section 3, we define more precisely the optical system model used in our numerical experiments. We consider both a Gaussian white noise and a fractal noise of unknown correlations generated by a standard technique of spectral synthesis. Section 4 is devoted to the position estimation problem, i.e. estimation of parameter ϵ . We propose two estimators that take into account the fact that the signal amplitude α is also unknown. We demonstrate the performance of these estimators in terms of mean square errors. As for the detection problem, we finally illustrate the expected improvement in quality brought by a correctly sampled optics compared to common sensor design.

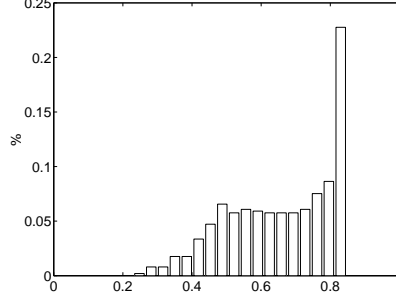


Fig. 2. Empirical distribution of the image-spot central pixel $s_\epsilon[0, 0]$ for a uniformly random position $\epsilon \sim \mathcal{U}_{[-0.5, 0.5]^2}$.

2. Detection problem

We consider a local detection window sliding across the image. The problem is to decide whether an object is present or not at the window central pixel. This is a binary test which typically reads as follows:

$$\begin{cases} H_0 & : \mathbf{z} = \mathbf{n} \\ H_1 & : \mathbf{z} = \alpha \mathbf{s}_\epsilon + \mathbf{n} \end{cases} \quad (2)$$

where \mathbf{z} is the vector collecting the window data, $\mathbf{s} = \alpha \mathbf{s}_\epsilon$ is the object response (signal vector) and \mathbf{n} the additive Gaussian noise. The signature shape is known and deterministic, so that \mathbf{s} only depends on the two unknown parameters $\alpha \in \mathbb{R}$ and $\epsilon \in \mathcal{E} = [-0.5, 0.5]^2$. The noise vector \mathbf{n} is supposed to be centered (in practice we first remove the empirical mean from the data) with a known or previously estimated covariance matrix \mathbf{R} . Thus, if we assume that \mathbf{n} is independent from \mathbf{s} , the following conditional distributions are Gaussian:

$$\begin{cases} p(\mathbf{z}|H_0) & \sim \mathcal{N}(\mathbf{0}, \mathbf{R}) \\ p(\mathbf{z}|H_1, \alpha, \epsilon) & \sim \mathcal{N}(\alpha \mathbf{s}_\epsilon, \mathbf{R}) \end{cases} \quad (3)$$

Let first assume that parameters α and ϵ are given. The problem amounts to a simple hypothesis test which is to detect a deterministic signal in a Gaussian noise. The Neyman-Pearson strategy or likelihood ratio test (LRT) is given by:

$$\frac{p(\mathbf{z}|H_1, \alpha, \epsilon)}{p(\mathbf{z}|H_0)} \underset{H_0}{\overset{H_1}{>}} \text{threshold} \quad (4)$$

It is equivalent to classical matched filtering which simply compares the statistic $\alpha \mathcal{T}_\epsilon(\mathbf{z}) = \alpha \mathbf{s}_\epsilon^t \mathbf{R}^{-1} \mathbf{z}$ with some threshold.

A. Pixel matched filtering

The exact object location being unknown in practice, we could assume by default that $\epsilon = \epsilon_0 = [0, 0]$, i.e. the object is at the center of the pixel, whereas the true location

would correspond to $\epsilon = \epsilon^*$. Thus, the detector which consists in thresholding the pixel matched filter (PMF) $\alpha \mathcal{T}_{\epsilon_0}(z)$ is optimum provided $\epsilon^* = \epsilon_0$. Otherwise it is mismatched and therefore suboptimum. Since conditional distributions of $\mathcal{T}_{\epsilon_0}(z)$ under each assumption are Gaussian, we easily get the expression of the probability of detection P_d and of false alarm P_{fa} . Corresponding receiver operating characteristic (ROC) curves for critical values of ϵ^* are depicted on Figure 3. They clearly show that the PMF performances are significantly worse as ϵ_0 differs from ϵ^* . But beyond extreme situations (related to a true target location between two or four pixels instead of the center), the “mean curve” represents the average statistics over uniformly random positions. Compared to the ideal curve, we can see that the price paid if one neglects the random location is rather high even at favorable signal-to-noise ratio. For a SNR of 15dB and at a P_{fa} of 10^{-4} , probability of detection decreases from nearly 1 to 0.8.

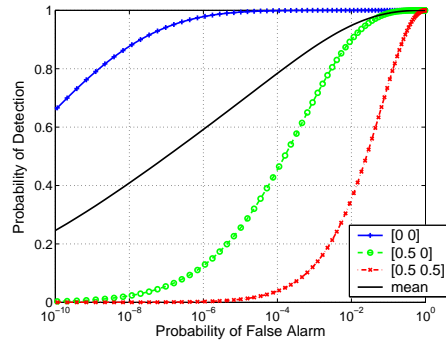


Fig. 3. Examples of pixel matched filter theoretical ROC curves for $\epsilon^* = \epsilon_0$ in blue (ideal curve), $\epsilon^* \neq \epsilon_0$ in green and red (worst case), and finally the mean curve in black for uniformly sampled ϵ^* (SNR = 15dB).

The object response also depends (linearly this time) on the amplitude α , which is generally unknown. Yet, assuming strictly positive amplitude, we see that whatever $\alpha > 0$, thresholding $\alpha \mathcal{T}_{\epsilon_0}(z)$ gives the same ROC curve as thresholding $\mathcal{T}_{\epsilon_0}(z)$. Without any assumption on α , a classical solution is to estimate it by maximum likelihood (ML). Indeed under the Gaussian noise assumption, the optimum in α for a given ϵ is explicit:

$$\begin{aligned}
 \hat{\alpha}(\epsilon) &= \arg \max_{\alpha \in \mathbb{R}} p(z|H_1, \alpha, \epsilon) \\
 &= \arg \min_{\alpha \in \mathbb{R}} \{ (z - \alpha s_\epsilon)^t \mathbf{R}^{-1} (z - \alpha s_\epsilon) \} \\
 &= \frac{s_\epsilon^t \mathbf{R}^{-1} z}{s_\epsilon^t \mathbf{R}^{-1} s_\epsilon}
 \end{aligned} \tag{5}$$

and then the “generalized” pixel matched filter (referred to as GPMF) is equal to

$$\hat{\alpha}(\epsilon_0) \mathcal{T}_{\epsilon_0}(z) = \frac{|s_{\epsilon_0}^t \mathbf{R}^{-1} z|^2}{s_{\epsilon_0}^t \mathbf{R}^{-1} s_{\epsilon_0}}. \tag{6}$$

B. Subpixel detectors

Our aim is to build refined detectors that improve performance of the above GPMF in taking into account the variability of the object signature due to its random subpixel location. Several solutions may be used. We first recall the most popular one.

1. Generalized likelihood ratio test

ML estimation of the two unknown parameters leads to the generalized likelihood ratio test (GLRT):

$$\begin{aligned}\mathcal{L}_g(\mathbf{z}) &= \frac{\max_{(\alpha, \epsilon)} p(\mathbf{z}|\mathbf{H}_1, \alpha, \epsilon)}{p(\mathbf{z}|\mathbf{H}_0)} \\ &= \frac{p(\mathbf{z}|\mathbf{H}_1, \hat{\alpha}_{\text{ML}}, \hat{\epsilon}_{\text{ML}})}{p(\mathbf{z}|\mathbf{H}_0)} \begin{matrix} > \\ < \end{matrix} \text{threshold}.\end{aligned}\tag{7}$$

It consists in estimating the amplitude α and the possible object location ϵ by computing:

$$\begin{aligned}\hat{\epsilon}_{\text{ML}} &= \arg \max_{\epsilon \in \mathcal{E}} p(\mathbf{z}|\mathbf{H}_1, \hat{\alpha}(\epsilon), \epsilon) \\ &= \arg \max_{\epsilon \in \mathcal{E}} \left\{ \frac{|\mathbf{s}_{\epsilon}^t \mathbf{R}^{-1} \mathbf{z}|^2}{\mathbf{s}_{\epsilon}^t \mathbf{R}^{-1} \mathbf{s}_{\epsilon}} \right\},\end{aligned}\tag{8}$$

then thresholding the estimated filter $\hat{\alpha}_{\text{ML}} \mathcal{T}_{\hat{\epsilon}_{\text{ML}}}(\mathbf{z})$ where $\hat{\alpha}_{\text{ML}} = \hat{\alpha}(\hat{\epsilon}_{\text{ML}})$ is given by equation (5):

$$\hat{\alpha}_{\text{ML}} \mathcal{T}_{\hat{\epsilon}_{\text{ML}}}(\mathbf{z}) = \frac{|\mathbf{s}_{\hat{\epsilon}_{\text{ML}}}^t \mathbf{R}^{-1} \mathbf{z}|^2}{\mathbf{s}_{\hat{\epsilon}_{\text{ML}}}^t \mathbf{R}^{-1} \mathbf{s}_{\hat{\epsilon}_{\text{ML}}}}.\tag{9}$$

2. Exact likelihood ratio test

In a Bayesian approach, we propose to consider the two unknown parameters α and ϵ as realizations of independent random variables with given probability density functions $p(\alpha)$ and $p(\epsilon)$. Then the optimal procedure is the exact likelihood ratio test (ELRT).

To compute the density function of data under \mathbf{H}_1 and to get the likelihood ratio, we have to integrate the conditional density $p(\mathbf{z}|\mathbf{H}_1, \alpha, \epsilon)$ over prior distributions of the nuisance random parameters α and ϵ . The likelihood ratio can be expressed as:

$$\mathcal{L}(\mathbf{z}) = \frac{p(\mathbf{z}|\mathbf{H}_1)}{p(\mathbf{z}|\mathbf{H}_0)} = \frac{\int_{\mathcal{E}} \int_{\mathbb{R}} p(\mathbf{z}|\mathbf{H}_1, \alpha, \epsilon) p(\alpha) p(\epsilon) d\alpha d\epsilon}{p(\mathbf{z}|\mathbf{H}_0)}.\tag{10}$$

Given prior distributions $p(\alpha)$ and $p(\epsilon)$, $\mathcal{L}(\mathbf{z})$ is the optimal Neyman-Pearson test whenever α and ϵ really satisfy the models $p(\alpha)$ and $p(\epsilon)$. By default we choose a “non-informative” prior for α and we adopt a uniform distribution inside the pixel for ϵ , which seems to be quite a reasonable assumption for the subpixel target position. So we get:

$$\mathcal{L}(\mathbf{z}) \propto \int_{\mathcal{E}} \frac{1}{\sqrt{\mathbf{s}_{\epsilon}^t \mathbf{R}^{-1} \mathbf{s}_{\epsilon}}} \exp \left\{ \frac{|\mathbf{s}_{\epsilon}^t \mathbf{R}^{-1} \mathbf{z}|^2}{2 \mathbf{s}_{\epsilon}^t \mathbf{R}^{-1} \mathbf{s}_{\epsilon}} \right\} d\epsilon.\tag{11}$$

Unfortunately, because of intricate nonlinear dependence of \mathbf{s}_{ϵ} on ϵ , explicit integration over ϵ appears to be not tractable and probability distribution of $\mathcal{L}(\mathbf{z})$ is not as simple as the one of $\mathcal{T}_{\epsilon_0}(\mathbf{z})$. A quadrature approximation is required to compute $\mathcal{L}(\mathbf{z})$ whereas derivation of its density requires Monte-Carlo simulations.

3. Approximate likelihood ratio test

In equation (11), the double integral over ϵ can be approximated up to any desired accuracy using some quadrature rule and evaluating the integrand $f(\epsilon|z)$ at discrete samples $\epsilon_k \in \mathcal{E} = [-0.5, 0.5]^2$. But, for sake of computational efficiency, we propose to use a coarsest approximation of the likelihood ratio (ALRT) based on a bidimensional trapezoidal rule which only involves the 9 half-pixel positions.

4. Subspace model

One alternative to this probabilistic viewpoint can be built on a geometric approach that restricts the signal vector $\mathbf{s} = \alpha \mathbf{s}_\epsilon$ to vary in some P -dimensional subspace, with P lower than the vector size.¹⁰ The observed data under H_1 are rewritten as:

$$\mathbf{z} \simeq \mathbf{S}\mathbf{a} + \mathbf{n} = \sum_{p=1}^P a_p \mathbf{s}_p + \mathbf{n}, \quad (12)$$

where the structural matrix \mathbf{S} is formed by P independent vectors \mathbf{s}_p . Coefficients a_p of the linear combination are the new parameters that describe the signal variability. Thanks to linearity, ML estimation of vector \mathbf{a} has an explicit solution (which is identical to the least squares estimator):

$$\hat{\mathbf{a}}_{\text{ML}} = (\mathbf{S}^t \mathbf{R}^{-1} \mathbf{S})^{-1} \mathbf{S}^t \mathbf{R}^{-1} \mathbf{z} \quad (13)$$

and GLRT amounts to threshold the following statistic:

$$\mathcal{D}(\mathbf{z}) = \mathbf{z}^t \mathbf{R}^{-1} \mathbf{S} (\mathbf{S}^t \mathbf{R}^{-1} \mathbf{S})^{-1} \mathbf{S}^t \mathbf{R}^{-1} \mathbf{z}. \quad (14)$$

Matrix \mathbf{S} only depends on ϵ , α being a scale parameter. In practice, it is identified by discretizing \mathcal{E} , making a singular value decomposition and retaining the singular vectors \mathbf{s}_p corresponding to the P greatest singular values. We choose $P = 1$ which gives better results than higher orders. Therefore under hypothesis H_1 , $\mathbf{z} \simeq a_1 \mathbf{s}_1 + \mathbf{n}$ and $\mathcal{D}(\mathbf{z})$ is identical to GPMF with \mathbf{s}_1 replacing \mathbf{s}_{ϵ_0} .

3. Application to optical imagery

A. Optical system

In our application, we can model the imaging system by a diffraction-limited, unaberrated optics with circular aperture and incoherent illumination.^{11,12} The object signal pattern \mathbf{s}_ϵ is then given by the integration of h_o on each pixel (see equation 1), where h_o is the radial point spread function (PSF) defined by the Airy disk:

$$h_o(u, v) = \frac{1}{\pi} \left[\frac{J_1(\pi \rho r_c)}{\rho} \right]^2, \quad \rho = \sqrt{u^2 + v^2}. \quad (15)$$

J_1 is the Bessel function of the first kind and $r_c = \nu_c / \nu_s$ designates the normalized cut-off frequency (ν_s is the sampling frequency and $\nu_c = D / \lambda$ is the radial cut-off frequency defined by the ratio of the lens aperture diameter D over the wavelength λ). Figure 4 depicts the two-dimensional PSF and a slice along one diameter, as well as their Fourier transform.

Common sensor design uses $r_c = 2.44$ so that the pixel size is equal to the width of the main lobe of the PSF. However, this implies a downsampling factor of $\nu_n/\nu_s = 2r_c = 4.88$ (where $\nu_n = 2\nu_c$ is the Nyquist frequency). In the following section, we present some numerical results of detection performance considering this classical sensor design. Examples of image spots \mathbf{s}_ϵ have been represented on Figure 1 for different values of ϵ .

Remark 1 *We have the following property:*

$$\sum_{(i,j) \in \mathbb{Z}^2} \mathbf{s}_\epsilon[i,j] = \int_{\mathbb{R}^2} h_o(u,v) du dv = 1.$$

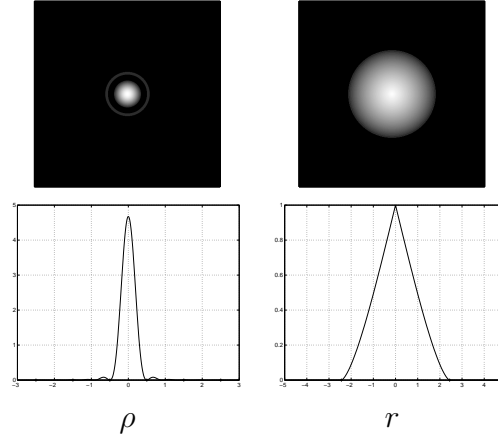


Fig. 4. *Left*: radial point spread function $h_o(u,v)$ on the top and slice along a diameter on the bottom. *Right*: corresponding optical transfer function $\tilde{h}_o(\nu_u, \nu_v)$ and slice along a diameter ($r_c = 2.44$).

B. Numerical results

Performances of the five classes of detectors have been compared in terms of ROC curves: GPMF, GLRT on α and ϵ , ELRT, ALRT and finally GLRT with the subspace model denoted SM-GLRT. Probabilities of detection and false alarm are deduced from the empirical distributions of these statistics under each hypothesis by generating samples of Gaussian noise \mathbf{n} and uniformly distributed ϵ in $\mathcal{E} = [-0.5, 0.5]^2$. The amplitude is assumed to be unknown but set to a constant value α in the simulations since we have no information about a reliable prior distribution $p(\alpha)$.

We first consider the case of a Gaussian white noise $\mathbf{n} \sim \mathcal{N}(0, \sigma^2)$. The signal-to-noise ratio is then defined by:

$$\text{SNR} = 10 \log_{10} \left(\frac{\alpha^2 E}{\sigma^2} \right) \quad (16)$$

$$\text{with } E = \int_{\mathcal{E}} \sum_{(i,j) \in \mathbb{Z}^2} (\mathbf{s}_\epsilon[i,j])^2 d\epsilon$$

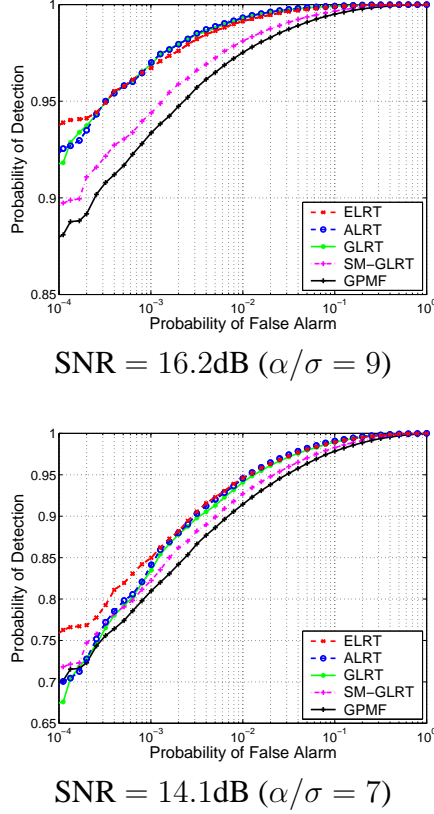


Fig. 5. Empirical ROC curves in the Gaussian white noise case with common sensor design ($r_c = 2.44$).

For common sensor design ($r_c = 2.44$), the average energy of the image spot is $E \simeq 0.52$. The ROC curves are depicted on Figure 5 for two different SNR. It shows that the GLRT, the ELRT (actually, a refined approximation of it) and the coarse approximation ALRT give significantly better performance than the SM-GLRT and GPMF. We also see that the performance gain is greater for high SNR whereas it tends to be rather small for low SNR and low probability of false alarm. Conversely, if the latter detectors are computationally cheap, including the ALRT, this is not so for the GLRT and the ELRT, which are much more intensive.

As complementary results, we have tested the five detectors on a fractal background image generated by a variant of the ppmforge software ¹. The synthesis algorithm depends on the auto-similarity parameter H called Hurst parameter and which is set to 0.7 in this experiment. The resulting image depicted on Figure 6 is a realistic simulation of a cloud scene. The covariance matrix \mathbf{R} of this stationary background is estimated by the empirical correlations on the whole image. We then compute the performance of the different detectors for a given target amplitude as illustrated on Figure 7. The ROC curves look quite

¹<http://h30097.www3.hp.com/demos/osscc/man-html/man1/ppmforge.1.html>

different from the white noise case but we notice again that the GLRT, ELRT and ALRT have similar performance and provide a significant detection gain in comparison with the GPMF or the SM-GLRT.

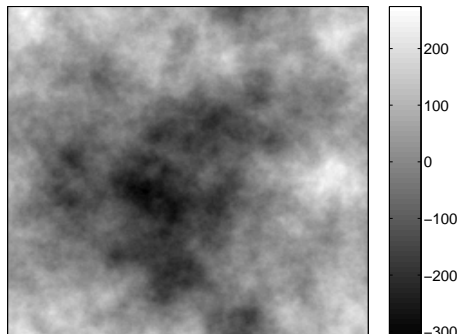


Fig. 6. Simulation of a cloud fractal image of 200×200 pixels (Hurst parameter $H = 0.7$).

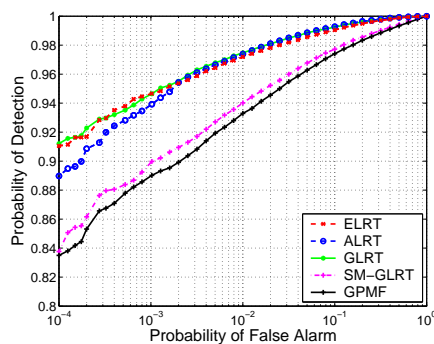


Fig. 7. Empirical ROC curves obtained on the fractal image of Figure 6 for a true (but assumed unknown) target amplitude $\alpha = 60$ gray levels.

C. Influence of the optics

Besides the perfecting and evaluation of subpixel detectors, one additional motivation of this work is to analyze the influence of aliasing on detection performance. This is the reason why we have also tested the detectors on a correctly sampled optics in order to compare their performances with those obtained using a common sensor design. In the correctly sampled design, the focal plane is sampled at Nyquist frequency (implying a denser sensor array or a smaller lens diameter) so that aliasing is suppressed. Parameter r_c of the PSF is equal to 0.5 and the signal energy is now spread over several pixels ($E \simeq 0.08$). By

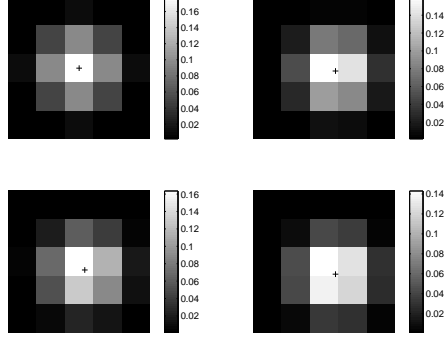


Fig. 8. Examples of image spots corresponding to a correctly sampled optics ($r_c = 0.5$) to be compared to those of Figure 1.

comparison, Figure 8 presents the examples of image spots corresponding to such a design. Detection performances are depicted on Figure 9 on the right for a SNR of 15dB. We see that improved detection has just a moderate impact in this situation. The five detectors have a quite similar behavior but at the same SNR they perform much better than in the aliased case. The gain in P_{fa} amounts at least to a factor 10 for all the detectors. Such a result speaks in favour of using a denser focal plane for point target detection.

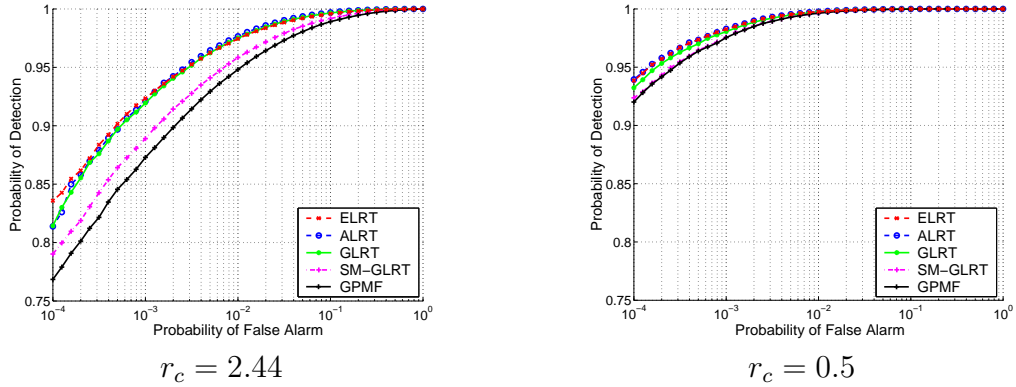


Fig. 9. Empirical ROC curves in the Gaussian white noise case for a same SNR = 15dB, with common sensor design on the left ($r_c = 2.44$) compared to a correctly sampled optics on the right ($r_c = 0.5$).

4. Performance of subpixel position estimators

Up to now we have focused on the detection strategy. In a second step, once a potential target is detected on a given pixel, we are also interested in accurate estimation of its subpixel

position. Such a problem has already been addressed, in particular for star position estimation in astronomical applications.¹³ Several types of estimators are possible. We consider here the maximum likelihood (ML) estimator and following the Bayesian approach introduced previously the posterior mean (PM). It is important to note that the signal amplitude α is also unknown and therefore we have to estimate it or integrate over it. Indeed it is not valid to suppose that the amplitude is known in the context of IRST.

The ML estimator of ϵ is given in equation (8) by replacing α with its estimate $\hat{\epsilon}$. Actually, $\hat{\epsilon}_{\text{ML}}$ and $\hat{\alpha}_{\text{ML}} = \hat{\alpha}(\hat{\epsilon}_{\text{ML}})$ are identical to joint maximum *a posteriori* (MAP) estimators with non-informative priors on the two parameters.

The PM estimator is defined as:

$$\hat{\epsilon}_{\text{PM}} = \int_{\mathcal{E}} \epsilon p(\epsilon | H_1, \mathbf{z}) d\epsilon \quad (17)$$

where the posterior law is deduced from Bayes' rule:

$$\begin{aligned} p(\epsilon | H_1, \mathbf{z}) &= \frac{p(\mathbf{z} | H_1, \epsilon) p(\epsilon)}{p(\mathbf{z} | H_1)} \\ &= \frac{p(\epsilon)}{p(\mathbf{z} | H_1)} \int_{\mathbb{R}} p(\mathbf{z} | H_1, \alpha, \epsilon) p(\alpha) d\alpha. \end{aligned} \quad (18)$$

So, we have to integrate over α and then over ϵ . As previously we consider a diffuse *a priori* on \mathbb{R} for α and a uniform law on \mathcal{E} for ϵ . We get the following expression in the same way as for the likelihood ratio in equation (11):

$$p(\epsilon | H_1, \mathbf{z}) \propto \frac{1}{\sqrt{\mathbf{s}_\epsilon^t \mathbf{R}^{-1} \mathbf{s}_\epsilon}} \exp \left\{ \frac{|\mathbf{s}_\epsilon^t \mathbf{R}^{-1} \mathbf{z}|^2}{2 \mathbf{s}_\epsilon^t \mathbf{R}^{-1} \mathbf{s}_\epsilon} \right\}. \quad (19)$$

We have studied the performance of these two estimators in terms of average mean square error (MSE). In practice, the optimization or the integration over ϵ are approximated numerically by considering a finite discrete grid of 20×20 values $\epsilon_k \in \mathcal{E}$. Given a true position ϵ^* , bias and variance of an estimator $\hat{\epsilon}$ are estimated thanks to Monte-Carlo simulations. We consider the case of a Gaussian white noise and we vary the signal-to-noise ratio. Figure 10 on the left compares ML and PM estimators to the pixel estimator which assumes by default that the target location is at the center of the pixel ($\hat{\epsilon} = (0, 0)$) and whose MSE is equal to $1/12$. At favorable SNR, the two subpixel estimators are far better than the default estimator but the gain decreases when the noise becomes important. For a SNR of 15dB, the ML yields an error similar to the default estimator while the PM notably has a twice smaller error. By comparison, Figure 10 on the right shows the estimation performances obtained in the unaliased case ($r_c = 0.5$) for equivalent signal-to-noise ratios. ML and PM logically perform better since the signal is correctly sampled.

5. Conclusion and future work

We have presented the detection problem of subpixel objects embedded in additive Gaussian noise. Subpixel location and signal amplitude are assumed to be unknown. Unknown subpixel location has a great influence on detection performance in the aliased case while

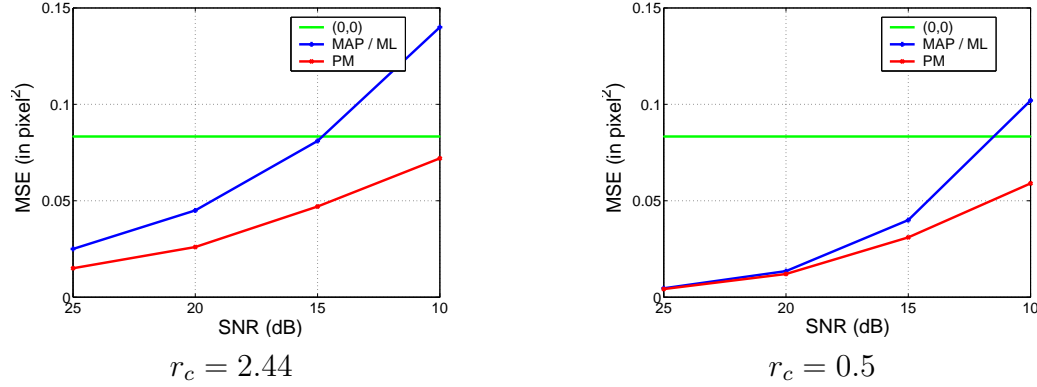


Fig. 10. Average mean square errors (MSE) of position estimators in the Gaussian white noise case with common sensor design on the left ($r_c = 2.44$) compared to a correctly sampled optics on the right ($r_c = 0.5$).

conventional matched filter neglects it. Thus, we derived four types of improved detectors from the likelihood ratio: the GLRT, the ELRT, the ALRT and the SM-GLRT. We have illustrated their performance in comparison with the more classical GPMF. Numerical results for both white and correlated noise cases show that the ELRT, the ALRT and the GLRT are competitive whereas the SM-GLRT does not reach the same quality but slightly improves the performance of the GPMF too. The ALRT seems to be a good trade-off since it is not as computationally demanding as the ELRT and the GLRT. Moreover the performance gain proves to be only moderate in the case of unaliased optics. This conclusion has important consequence in sensor design: it suggests that the popular design of a pixel covering exactly the main lobe of the Airy disk is not optimum for point object detection. Future work consists in studying the robustness of these detectors to real data and the way we can take into account non Gaussian distributions of background noise. As far as the position estimation problem is concerned, we have demonstrated prospective gains that must also be confirmed on more realistic data.

References

1. C. D. Wang, "Adaptive spatial/temporal/spectral filters for background clutter suppression and target detection," *Optical Engineering*, vol. 21, pp. 1033–1038, Dec. 1982.
2. A. Margalit, I. S. Reed, and R. M. Gagliardi, "Adaptive optical target detection using correlated images," *IEEE Transactions on Aerospace and Electronic Systems*, vol. 21, pp. 394–405, May 1985.
3. T. Soni, J. R. Zeidler, and W. H. Ku, "Performance evaluation of 2-D adaptive prediction filters for detection of small objects in image data," *IEEE Transactions on Image Processing*, vol. 2, pp. 327–340, July 1993.
4. X. Yu, L. E. Hoff, I. S. Reed, A. M. Chen, and L. B. Stotts, "Automatic target detection and recognition in multiband imagery : a unified ML detection and estimation

- approach,” *IEEE Transactions on Image Processing*, vol. 6, pp. 143–156, Jan. 1997.
5. E. A. Ashton, “Detection of subpixel anomalies in multispectral infrared imagery using an adaptive Bayesian classifier,” *IEEE Transactions on Geoscience and Remote Sensing*, vol. GE-36, pp. 506–517, Mar. 1998.
 6. I. S. Reed, R. M. Gagliardi, and H. M. Shao, “Application of three-dimensional filtering to moving target detection,” *IEEE Transactions on Aerospace and Electronic Systems*, vol. 19, pp. 898–905, Nov. 1983.
 7. S. D. Blostein and T. S. Huang, “Detecting small, moving objects in image sequences using sequential hypothesis testing,” *IEEE Transactions on Signal Processing*, vol. 39, pp. 1611–1629, July 1991.
 8. J. M. Mooney, J. Silverman, and C. E. Caefer, “Point target detection in consecutive frame staring infrared imagery with evolving cloud clutter,” *Optical Engineering*, vol. 34, pp. 2772–2784, Sept. 1995.
 9. H. L. Van Trees, *Detection, estimation and modulation theory*. Part1, New York: Wiley, John, 1968.
 10. D. Manolakis and G. Shaw, “Detection algorithms for hyperspectral imaging applications,” *Signal Processing Magazine*, vol. 19, pp. 29–43, Jan. 2002.
 11. J. W. Goodman, *Introduction à l’optique de Fourier et à l’holographie*. Paris: Masson, 1972.
 12. R. C. Hardie, K. J. Barnard, J. G. Bognar, E. E. Armstrong, and E. A. Watson, “High-resolution image reconstruction from a sequence of rotated and translated frames and its application to an infrared imaging system,” *Optical Engineering*, vol. 37, pp. 247–260, Jan. 1998.
 13. K. A. Winick, “Cramer-Rao lower bounds on the performance of charge-coupled-device optical position estimators,” *Journal of the Optical Society of America A*, vol. 3, pp. 1809–1815, Nov. 1986.